Searching for Chameleon Dark Energy with Mechanical Systems

J. Betz,[1] J. Manley,[2] E. M. Wright,[3] D. Grin,[4] and S. Singh[2,1,*]
[1]Department of Physics and Astronomy, University of Delaware, Newark, Delaware 19716, USA
[2]Department of Electrical and Computer Engineering, University of Delaware, Newark, Delaware 19716, USA
[3]Wyant College of Optical Sciences, University of Arizona, Tucson, Arizona 85721, USA
[4]Department of Physics and Astronomy, Haverford College, Haverford, Pennsylvania 19041, USA

(Received 10 February 2022; revised 20 July 2022; accepted 29 August 2022; published 23 September 2022)

A light scalar field framework of dark energy, sometimes referred to as quintessence, introduces a fifth force between normal matter objects. Screening mechanisms, such as the chameleon model, allow the scalar field to be almost massless on cosmological scales while simultaneously evading laboratory constraints. We explore the ability of existing mechanical systems to directly detect the fifth force associated with chameleons in an astrophysically viable regime where it could be dark energy. We provide analytical expressions for the weakest accessible chameleon model parameters in terms of experimentally tunable variables and apply our analysis to two mechanical systems: levitated microspheres and torsion balances, showing that the current generation of these experiments have the sensitivity to rule out a significant portion of the proposed chameleon parameter space. We also indicate regions of theoretically well-motivated chameleon parameter space to guide future experimental work.

DOI: 10.1103/PhysRevLett.129.131302

Introduction.—Multiple cosmological measurements [1–4] indicate the presence of a novel negative-pressure fluid with a constant energy density that dominates the energy budget of the Universe during the present epoch [5]. There is no consensus on the theoretical framework for the composition, properties, or production mechanism of this fluid, known as dark energy (DE), which could be responsible for the observed accelerated expansion of the Universe [6,7]. Theoretical approaches for building a DE framework typically involve the introduction of light scalar fields or modifications to general relativity [5–8]. In order to explain the observed cosmic acceleration, both scenarios must contend with new degrees of freedom mediating long-range forces between standard model (SM) particles. A variety of experiments have placed tight constraints on the long-range fifth force between SM particles due to such scalar fields. These constraints can be evaded by a class of theories known as "screened-scalar" models [7,9–17] such as the chameleon model.

In the chameleon model, the effective mass of the chameleon field is dynamically modified by terms that depend on the local matter density [7,10,18]. This allows the scalar field to remain light on cosmic scales, yet heavy in laboratory environments, where screening suppresses the fifth force, evading detection. The strong dependence on the local matter density causes the chameleon field and corresponding force between two objects to be extremely sensitive to the local geometry and surrounding environment.

Supplementing observational constraints on screened-scalar models [19–29], the best laboratory constraints on the chameleon model come from the Eöt-Wash torsion pendulum [30,31] and atom interferometry experiments [32]. The Eöt-Wash torsion pendulum is able to position large source and test masses with micron separations, providing excellent constraints on scalar field mediated forces. However, these large masses make it difficult to probe stronger chameleon coupling strengths because of screening. Atom interferometry experiments can access a complementary chameleon parameter space using smaller test masses. However, they are limited to stronger coupling strengths because the small masses result in a correspondingly small chameleon force. Precision measurement experiments with intermediate size masses are uniquely

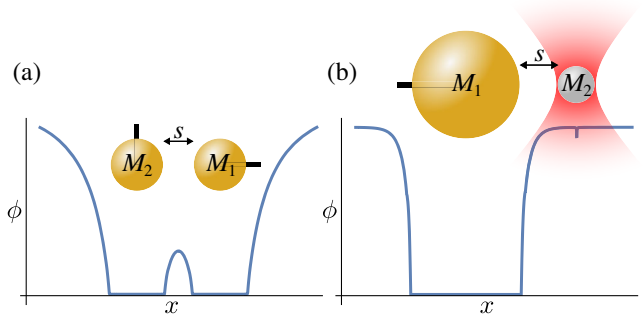

FIG. 1. Schematic of mechanical systems considered here to detect the chameleon mediated force between matter. In both cases, M_1 is the gold source mass, while M_2 is the mechanically compliant test mass. We consider (a) torsion balance and (b) optically levitated microspheres as sensors of chameleon DE. The blue curves show the two-body chameleon field profile. The levitated microsphere is enlarged to show detail.

 © 2022 American Physical Society

suited to fill the resulting gap in the existing chameleon constraints. However, there is little theoretical guidance to help design such experiments, particularly targeting the astrophysically viable regime where the coupling between chameleons and normal matter is comparable to or weaker than that due to gravity.

In this Letter, we present a theoretical treatment of mechanical systems as sensors of the fifth force associated with chameleon DE. Considering spherically symmetric masses, we provide analytical expressions for the weakest accessible chameleon field phenomenology parameters (such as the self-interaction strength and coupling to normal matter) in terms of experimental parameters such as size, distance between spheres, and the minimum detectable force. Our expressions provide a straightforward pathway to estimate the performance of existing devices and scaling arguments useful for design considerations of future devices, without the need for numerically intensive solutions.

We then discuss two classes of spherical mechanical systems: levitated microspheres and Cavendish-style torsion balances. Both systems have demonstrated exceptional sensitivity to weak forces [33–35] and there has been some work considering microspheres as potential probes for scalar and screened-scalar fields [36–39]. Using a novel analytical treatment allowing us to consider systems with larger masses, we show that for both mechanical systems, the current generation of experiments have the sensitivity to put new constraints in a region of interest to cosmology, possibly ruling out chameleons as DE. We also present the region of phenomenologically motivated chameleon DE parameter space that future experiments could be optimized to target.

Chameleon model.—The chameleon force between two objects of masses M_1 and M_2 can be approximated by [40,41]

$$F_{\rm cham}(x) = 2\alpha \frac{GM_1M_2}{x^2}\lambda_1\lambda_2\left(\frac{M_p}{M}\right)^2, \tag{1}$$

where M is the chameleon-matter coupling, M_p is the reduced Planck mass, x is the center of mass separation distance, $\lambda_{1,2}$ are the chameleon screening factors associated with each object, and α is a dimensionless factor (see below). The screening factors are given by [41]

$$\lambda_i = \begin{cases} 1, & \rho_i R_i^2 < 3M\phi_{\rm bg}, \\ \approx \dfrac{3M\phi_{\rm bg}}{\rho_i R_i^2}, & \rho_i R_i^2 > 3M\phi_{\rm bg}, \end{cases} \tag{2}$$

where $\phi_{\rm bg} = (nM\Lambda^{4+n}/\rho_{\rm bg})^{1/(n+1)}$ is the background value of the chameleon field, R_i and ρ_i are the radius and density of the object. The background field value $\phi_{\rm bg}$ depends on the background density $\rho_{\rm bg}$, the chameleon self-interaction coupling Λ, and the power-law index n. The coupling parameters M, Λ, and n, which come from the chameleon equation of motion,

$$\nabla^2\phi = -\frac{\Lambda^{4+n}}{\phi^{n+1}} + \frac{\rho}{M}, \tag{3}$$

are the three independent parameters of the chameleon model. As Eq. (2) demonstrates, with all other parameters held fixed, a larger or more dense object will be screened more relative to a smaller, less dense one. Additionally, increasing the density surrounding an object will cause more screening. It is this screening mechanism which prevents observations of the chameleon force between macroscopic objects.

The chameleon force between two objects derived in Refs. [39–41] assumes a mass hierarchy between the source and test mass such that the two-body field solution can be approximated by a superposition of the respective one-body solutions. We found that when both masses are of a similar scale, this approximation breaks down. However, this similar scale regime is of interest because, as shown below, experiments operating in this regime can be used to set new bounds on the chameleon parameter space.

In order to derive an expression for the chameleon force that does not assume a mass hierarchy, we start with a new ansatz approximating the two-body field solution as the product of the one-body solutions, $\phi(\mathbf{x}) \approx \phi_1(\mathbf{x}-\mathbf{x}_1)\phi_2(\mathbf{x}-\mathbf{x}_2)/\phi_{\rm bg}$. This approximation bridges the gap in parameter space where the assumption of approximate linearity in the equation of motion and two-body solution breaks down. Instead, we choose to approximately balance the nonlinear term with the source terms as the zeroth order approximation which yielded the multiplicative form of the ansatz (see Supplemental Material for more details [42]). Taking the same approximations used in Ref. [41], we found a force expression that matched the previous result ($\alpha = 1$) [39–41] except in the regime where both spheres are strongly perturbing. In this case, our force is smaller by a factor of $\alpha = 1/6$. To ensure the validity of the proposed constraints below, the multiplicative ansatz was compared with the numerical field solution over the entire parameter space probed by the proposed torsion balance system.

First, we consider chameleon DE models by fixing $\Lambda = \Lambda_{\rm DE} \sim 2.4 \times 10^{-3}$ eV [3]. The free parameters are the chameleon-matter coupling M and the power-law index n. For laboratory scale experiments with a minimum force sensitivity $F_{\rm min}$, setting $F_{\rm cham} = F_{\rm min}$ yields an analytic expression for the maximum M value that can be probed by the experiment,

$$\frac{M_{\rm max}}{M_p} = \left(\frac{32\pi^2}{9}\frac{G\rho_1\rho_2}{F_{\rm min}}\frac{R_1^3R_2^3}{(s+R_1+R_2)^2}\right)^{1/2}. \tag{4}$$

All parameters on the right side of the equation are in Systeme International (SI) units including the surface separation distance s. The minimum detectable force $F_{\rm min}$ may depend on the radius of the test mass. Where $M = M_{\rm max}$, both the source and test mass are unscreened ($\lambda_{1,2} = 1$) and the chameleon force is independent of n and Λ. Additionally, the maximum n value can be found numerically by solving the following equation,

$$F_{\rm min} = 4\pi\xi^2 \frac{R_1 R_2}{(s + R_1 + R_2)^2} \left(\frac{1}{\hbar c}\right)^{(n_{\rm max}+6)/(n_{\rm max}+2)} \times [n_{\rm max}(n_{\rm max}+1)(\Lambda_{\rm DE})^{4+n_{\rm max}} L^2]^{\frac{2}{n_{\rm max}+2}}. \quad (5)$$

Here, all parameters are in SI units. The dimensionless factor ξ is a constant which characterizes the geometry of the vacuum chamber. For a spherical vacuum chamber of radius L, $\xi = 0.55 - 0.68$, which was found numerically in Ref. [44] in addition to other vacuum chamber geometries.

Beyond dark energy (i.e., $\Lambda \neq \Lambda_{\rm DE}$), chameleon screening could hide scalar fields appearing in string theory inspired scenarios beyond the standard model [45,46]. Focusing on $n \geq 1$, analytic expressions can be found for the maximum M and minimum Λ values that can be probed by a particular experiment. $M_{\rm max}$ is given by Eq. (4) and $\Lambda_{\rm min}$ by

$$\Lambda_{\rm min} = \left(\frac{F_{\rm min}}{4\pi\xi^2} \frac{(s + R_1 + R_2)^2}{R_1 R_2}\right)^{3/10} \left(\frac{1}{L}\right)^{2/5} \frac{(\hbar c)^{7/10}}{1.6 \times 10^{-19}}. \quad (6)$$

Here, Λ is in eV, and all parameters on the right side of the equation are in SI units.

Experiment.—Figure 1 illustrates a simplified schematic for a general fifth force experiment. The force between two masses is inferred by measuring the position of a test mass M_2 (modeled as a harmonic oscillator) with radius R_2, in response to the force exerted on it by a source mass M_1 with radius R_1. The position of the source mass is made to oscillate to avoid low frequency noise, resulting in an oscillating force signal $F(t)$ on the test mass. With resonant amplification and sufficiently low-noise displacement readout, a force measurement will be limited by thermomechanical noise in the oscillator.

A harmonic oscillator with dissipation Γ_0 and effective mass m_0, operating at a finite temperature T, will have a thermal force noise spectrum $S_{FF}^{\rm th}(f) = 4k_B T m_0 \Gamma_0$. We have approximated the force signal as monochromatic, and the signal to noise ratio for a coherent signal over stochastic noise can be improved by averaging down the variance in the noise floor over a longer measurement time τ, so that the thermally limited minimum detectable force is

$$F_{\rm min} \approx \sqrt{2S_{FF}^{\rm th}/\tau} = \sqrt{8k_B T m_0 \Gamma_0/\tau}. \quad (7)$$

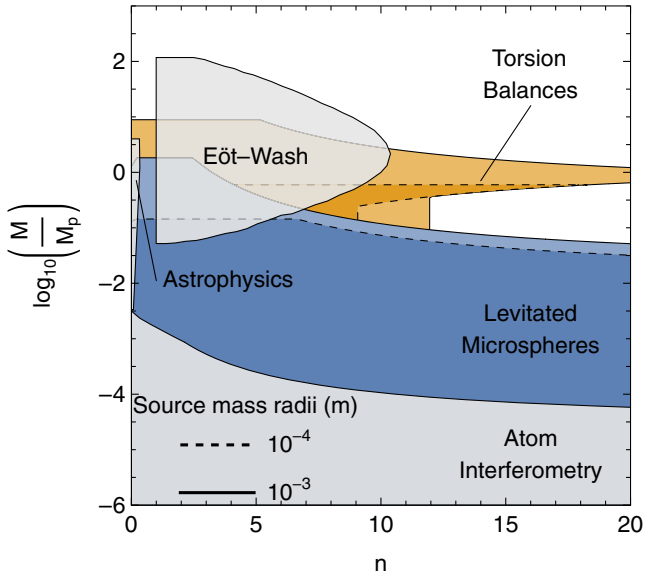

FIG. 2. Projected constraints from levitated microspheres (blue) and torsion balances (orange) as chameleon dark energy detectors, where the chameleon self-coupling is fixed at $\Lambda = \Lambda_{\rm DE}$. In this plot, we consider a microsphere system with $R_1 = 5$ μm, $s = 0.5$ mm, and $F_{\rm min} = 10^{-21}$ N, and a torsion balance system with $R_1 = 0.1$ mm, $s = 0.6$ mm, and $F_{\rm min} = 4 \times 10^{-18}$ N. For both systems, the solid (dashed) black line corresponds to source a mass with $R_1 = 1$ mm (0.1 mm). The multiplicative ansatz and force expression are used to generate the torsion balance curves in the region where the additive ansatz breaks down. Existing constraints from Ref. [16], which include results from Refs. [24,26,30,32], are shown in gray. See Ref. [42] for a qualitative description of chameleon constraint plots.

While this expression holds irrespective of the source or test mass geometries, we consider the specific case of spherical masses, for which an analytical expression for the force due to a chameleon field is provided by Eq. (1).

Multiple existing force sensors with spherical test masses are capable of performing thermally limited force measurements, achieving low enough sensitivities to probe chameleon dark energy models [31,35,47–51]. In Figs. 2 and 3, we plot the estimated constraints that can be set on chameleon models by two classes of sensors: optically levitated microspheres and torsion balances.

The blue shaded regions in Figs. 2 and 3 demonstrate the estimated reach of levitated microspheres, where the test mass is a silica sphere with radius $R_2 = 5$ μm that is confined within a harmonic potential via optical trapping. Such sensors operating in high vacuum have been shown to achieve attonewton/$\sqrt{\rm Hz}$ force sensitivities [50]. For simplicity, we assume gas damping (due to collisions with the surrounding gas molecules) as the dominant dissipation mechanism giving rise to thermomechanical noise. In a vacuum chamber at pressure 10^{-6} mbar and temperature $T = 300$ K, we estimate $\Gamma_0 \approx 10^{-4}$ s^{-1} from an expression in Ref. [37] for gas damping. This yields a thermally

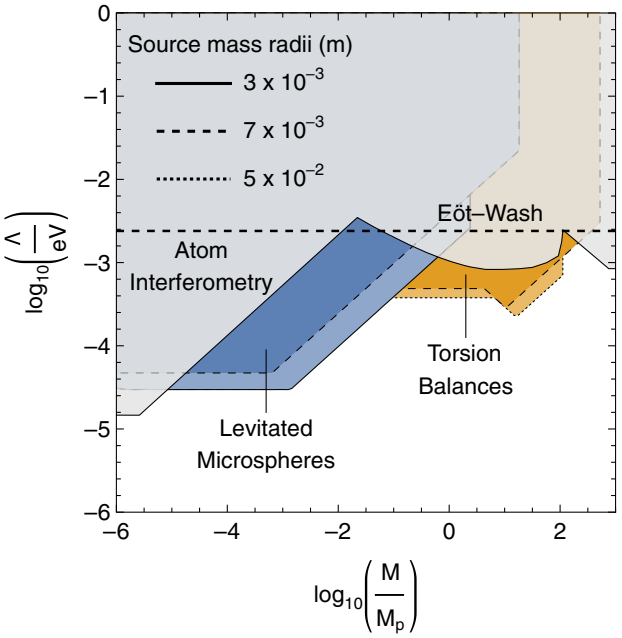

FIG. 3. Projected constraints from levitated microspheres (blue) and torsion balances (orange) as chameleon dark energy detectors, where the power-law index is fixed at $n = 1$. In this plot, we consider a microsphere system with $R_2 = 5$ μm, $s = 3$ mm, and $F_{\rm min} = 10^{-21}$ N, and a torsion balance system with $R_2 = 1$ mm, $s = 6$ mm, and $F_{\rm min} = 10^{-16}$ N. For torsion balances, the dashed (dotted) black line corresponds to a source mass with $R_1 = 7$ mm (5 cm). The multiplicative ansatz and force expression are used to generate the torsion balance curves in the region where the additive ansatz breaks down. For microspheres, the solid (dashed) black line corresponds to a source mass with $R_1 = 3$ mm (7 mm). The horizontal black dashed line indicates the dark energy scale $\Lambda = \Lambda_{\rm DE}$. Existing constraints from Ref. [16], which include results from Refs. [30,32], are shown in gray.

limited force sensitivity of 10^{-18} N$/\sqrt{\rm Hz}$, and a minimum detectable force of 10^{-21} N for a $\tau = 2$ week measurement.

To supplement the projected constraints from levitated microspheres, we also consider torsion balances, whose larger test masses enable them to probe weaker chameleon-matter couplings (larger M). A simple Cavendish-style torsion balance [35] consists of equally sized spheres, connected by a rod of negligible mass, which is suspended at its center by a torsion fiber and placed in a vacuum chamber. One of the spheres serves as the test mass M_2, while the balance as a whole forms a harmonic oscillator with effective mass $m_0 \approx 2M_2$ and quality factor $Q_0 = 2\pi f_0/\Gamma_0$. Westphal *et al.* [35] have demonstrated that such torsion balances have the ability to make measurements near the thermal limit, achieving piconewton$/\sqrt{\rm Hz}$ force sensitivity. In Figs. 2 and 3, the orange regions correspond to the estimated constraints that can be set on chameleon models by torsion balances operating at pressure 10^{-6} mbar and temperature $T = 300$ K, assuming a quality factor of $Q_0 = 10$ and a torsional resonance frequency of $f_0 = 5$ mHz. In Fig. 2 (Fig. 3) we consider a gold test mass $R_2 = 0.1$ mm ($R_2 = 1$ mm), achieving a thermally limited force sensitivity of 4×10^{-15} N$/\sqrt{\rm Hz}$ (10^{-13} N$/\sqrt{\rm Hz}$) and a minimum detectable force of 4×10^{-18} N (10^{-16} N) for a $\tau = 2$ week measurement.

For both systems, we assume gold source masses, with various radii labeled in Figs. 2 and 3. The surface separation distances s between the test and source masses (see figure captions for values) are chosen such that Casimir forces are negligible relative to $F_{\rm min}$.

A common component in torsion balance experiments is an electromagnetic shield placed between the source and test masses [31,35]. These shields can also be used to control Casimir forces which are relevant for the geometries proposed here [39,52]. However, this shield will introduce further screening of the chameleon force which can be estimated analytically [30] or calculated numerically.

These experimental limitations can be overcome through better force sensitivity or improved design. For example, integration times upward of 1 month can be achieved presently [50] or in the near future for these systems. For fixed s and R_2, $M_{\rm max}$ is a monotonically increasing function of R_1, indicating that larger source masses are needed to probe weaker chameleon-matter coupling strengths. However, when fixing the same parameters, $\Lambda_{\rm min}$ can be minimized by a particular choice for R_1. This behavior is illustrated in Fig. 3; $\Lambda_{\rm min}$ has been optimized for the light blue and light orange regions by varying R_1 with fixed s and R_2.

It is important to note that the geometries proposed here do not set new constraints for unscreened scalar fields (Yukawa 5th forces). Unscreened scalar fields can evade experimental detection only through their large masses and subsequent exponential suppression which results in an extremely short range force. Thus, in order to detect these scalars, large masses at very small separation distances are required. Screened scalars, on the other hand, are generally very light in low density regions and can therefore have a significantly longer range force which scales as $1/r^2$. Rather than small separation distances, the key in designing experiments to search for screened scalars is to prevent screening of the source and test masses. This can be controlled by various parameters such as density, geometry, and size of the source and test masses, as well as the vacuum chamber size and pressure.

Cosmological and naturalness constraints.—Beyond the addition of a new force, introducing a new particle to the standard model can impact cosmological models and physics in the early Universe. For example, in Ref. [53] it was shown that for sufficiently strong matter-coupling (small M), the chameleon may disrupt big bang nucleosynthesis. For chameleons with matter couplings weaker than $\log_{10}(M/M_p) \gtrsim -0.26$, this breakdown can be avoided only for certain initial conditions [53]. Requiring the chameleon to behave as vacuum energy in

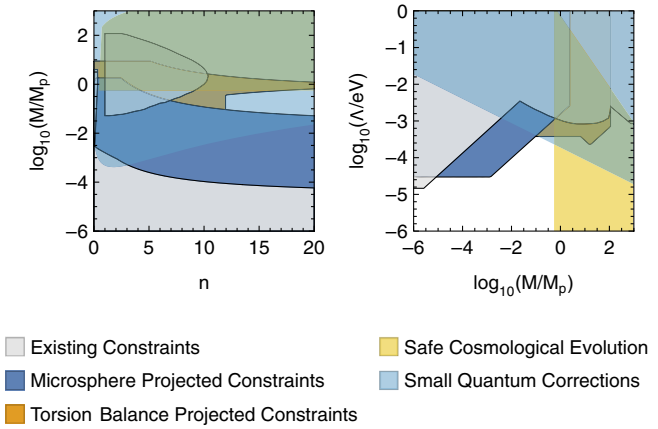

FIG. 4. The parameter space for both $n = 1$ and $n > 1$ chameleon models considered here is limited by cosmological [11,53,55] as well as quantum field theory analyses [56]. The green regions indicate where the chameleon model has safe cosmological evolution and small quantum corrections and should be the aim of future experimental searches. Existing and projected constraints from Figs. 2 and 3 are also shown. See Ref. [42] for region definitions.

the current epoch places a bound on the weakest allowable matter-coupling. In Ref. [11] it was shown that the chameleon will follow an attractor solution provided the condition $m^2/H^2 \gg 1$, where m is the chameleon mass and H is the Hubble parameter. For fixed n and Λ, this places a bound on the maximum value of M. Thus, only a particular region of parameter space is cosmologically well motivated with small quantum corrections. The range of parameter space satisfying both these constraints is indicated by the green region in Fig. 4. However, modified chameleon models such as the Dirac-Born-Infeld chameleon [15,54] may be feasible outside of this restricted parameter space.

As indicated in Fig. 4, the projected constraints for the systems considered here overlap significantly with the green region of interest. Such experiments can be further optimized using Eqs. (4)–(6). For instance, using a larger test mass would allow probing deeper into the green region in Fig. 4. This may be accomplished via magnetic levitation of the test mass [57–60], albeit with design considerations to avoid technical noise and screening due to the nearby matter. However, such a complicated geometry would necessarily require a numerical approach as the presence of additional nearby matter would invalidate the analytic treatment considered here.

Conclusion.—Current generation mechanical systems have the sensitivity to rule out significant portions of chameleon parameter space and cast doubt on the feasibility of chameleon dark energy. For inverse power-law models, only weakly coupled (gravitational strength) chameleons have viable early cosmological evolution [53]. On the other hand, it has been shown that the $n = -4$ model is cosmologically safe [61]. Future work will extend predicted constraints for these mechanical systems to negative n chameleon models and other screened scalar fields. We will also explore using mechanical systems with reduced geometries (such as disks, membranes, or strings), as DE detectors as the chameleon force may be enhanced between nonspherical objects [62].

Beyond DE and modified gravity theories, screening mechanisms can also be utilized to hide scalar fields coming from string theory. Mechanical systems are particularly well suited to search for such screened-scalar fields. Size, geometry, and material flexibility coupled with excellent force sensitivity makes them an ideal experimental platform for optimized searches for a variety of screening mechanisms.

We would like to thank Brian LaRocca and Mark Mirotznik for assistance with numerical simulations and Natalie Schmidt for assistance with figures. We also acknowledge helpful discussions with Jiyan Sang, Ryan Petery, Andy Geraci, Keith Schwab, Pierre Meystre, Markus Aspelmeyer, and David Moore. This work is supported by the National Science Foundation Grant No. PHY-2112846, No. PHY-1912480, No. PHY-2047707, and the Provost's Office at Haverford College.

*swatis@udel.edu

[1] A. G. Riess *et al.*, Astron. J. **116**, 1009 (1998).
[2] S. Perlmutter *et al.*, Astrophys. J. **517**, 565 (1999).
[3] N. Aghanim *et al.*, Astron. Astrophys. **641**, A6 (2020).
[4] S. Alam *et al.* (eBOSS Collaboration), Phys. Rev. D **103**, 083533 (2021).
[5] P. J. Steinhardt and N. Turok, Science **312**, 1180 (2006).
[6] R. R. Caldwell and M. Kamionkowski, Annu. Rev. Nucl. Part. Sci. **59**, 397 (2009).
[7] P. Brax, Rep. Prog. Phys. **81**, 016902 (2018).
[8] A. Joyce, L. Lombriser, and F. Schmidt, Annu. Rev. Nucl. Part. Sci. **66**, 95 (2016).
[9] J. Khoury and A. Weltman, Phys. Rev. D **69**, 044026 (2004).
[10] J. Khoury and A. Weltman, Phys. Rev. Lett. **93**, 171104 (2004).
[11] P. Brax, C. van de Bruck, A.-C. Davis, J. Khoury, and A. Weltman, Phys. Rev. D **70**, 123518 (2004).
[12] J. Khoury, arXiv:1011.5909.
[13] K. Hinterbichler, J. Khoury, A. Levy, and A. Matas, Phys. Rev. D **84**, 103521 (2011).
[14] P. Brax, Phys. Rev. D **90**, 023505 (2014).
[15] C. Burrage and J. Khoury, Phys. Rev. D **90**, 024001 (2014).
[16] C. Burrage and J. Sakstein, Living Rev. Relativity **21**, 1 (2018).
[17] C. Burrage, B. Coltman, A. Padilla, D. Saadeh, and T. Wilson, J. Cosmol. Astropart. Phys. 02 (2021) 050.
[18] K. Hinterbichler and J. Khoury, Phys. Rev. Lett. **104**, 231301 (2010).
[19] P. Brax, C. van de Bruck, A.-C. Davis, and A. M. Green, Phys. Lett. B **633**, 441 (2006).
[20] R. Bean, E. E. Flanagan, and M. Trodden, New J. Phys. **10**, 033006 (2008).
[21] R. Bean, E. E. Flanagan, and M. Trodden, Phys. Rev. D **78**, 023009 (2008).

[22] P. Brax, C. van de Bruck, A.-C. Davis, B. Li, B. Schmauch, and D. J. Shaw, Phys. Rev. D **84**, 123524 (2011).
[23] A.-C. Davis, B. Li, D. F. Mota, and H. A. Winther, Astrophys. J. **748**, 61 (2012).
[24] B. Jain, V. Vikram, and J. Sakstein, Astrophys. J. **779**, 39 (2013).
[25] P. Brax, A.-C. Davis, and R. Jha, Phys. Rev. D **95**, 083514 (2017).
[26] V. Vikram, J. Sakstein, C. Davis, and A. Neil, Phys. Rev. D **97**, 104055 (2018).
[27] C. A. J. O'Hare and C. Burrage, Phys. Rev. D **98**, 064019 (2018).
[28] A. Tamosiunas, C. Briddon, C. Burrage, W. Cui, and A. Moss, J. Cosmol. Astropart. Phys. 04 (2022) 047.
[29] M. Lagos and H. Zhu, J. Cosmol. Astropart. Phys. 06 (2020) 061.
[30] A. Upadhye, Phys. Rev. D **86**, 102003 (2012).
[31] D. J. Kapner, T. S. Cook, E. G. Adelberger, J. H. Gundlach, B. R. Heckel, C. D. Hoyle, and H. E. Swanson, Phys. Rev. Lett. **98**, 021101 (2007).
[32] M. Jaffe, P. Haslinger, V. Xu, P. Hamilton, A. Upadhye, B. Elder, J. Khoury, and H. Müller, Nat. Phys. **13**, 938 (2017).
[33] C. Montoya, E. Alejandro, W. Eom, D. Grass, N. Clarisse, A. Witherspoon, and A. A. Geraci, Appl. Opt. **61**, 3486 (2022).
[34] G. Ranjit, M. Cunningham, K. Casey, and A. A. Geraci, Phys. Rev. A **93**, 053801 (2016).
[35] T. Westphal, H. Hepach, J. Pfaff, and M. Aspelmeyer, Nature (London) **591**, 225 (2021).
[36] A. D. Rider, D. C. Moore, C. P. Blakemore, M. Louis, M. Lu, and G. Gratta, Phys. Rev. Lett. **117**, 101101 (2016).
[37] A. A. Geraci, S. B. Papp, and J. Kitching, Phys. Rev. Lett. **105**, 101101 (2010).
[38] C. P. Blakemore, A. Fieguth, A. Kawasaki, N. Priel, D. Martin, A. D. Rider, Q. Wang, and G. Gratta, Phys. Rev. D **104**, L061101 (2021).
[39] S. Qvarfort, D. Rätzel, and S. Stopyra, New J. Phys. **24**, 033009 (2022).
[40] L. Hui, A. Nicolis, and C. W. Stubbs, Phys. Rev. D **80**, 104002 (2009).
[41] C. Burrage, E. J. Copeland, and E. Hinds, J. Cosmol. Astropart. Phys. 03 (2015) 042.
[42] See Supplemental Material at http://link.aps.org/supplemental/10.1103/PhysRevLett.129.131302 for a qualitative description of chameleon constraint plots, details regarding the approximate two-body field solution, chameleon force derivation, and "safe" chameleon parameter space, which includes Ref. [43].
[43] P. Brax and S. Fichet, Phys. Rev. D **99**, 104049 (2019).
[44] P. Hamilton, M. Jaffe, P. Haslinger, Q. Simmons, H. Müller, and J. Khoury, Science **349**, 849 (2015).
[45] T. Damour and A. M. Polyakov, Nucl. Phys. **B423**, 532 (1994).
[46] P. Brax, C. van de Bruck, A.-C. Davis, and D. Shaw, Phys. Rev. D **82**, 063519 (2010).
[47] J. G. Lee, E. G. Adelberger, T. S. Cook, S. M. Fleischer, and B. R. Heckel, Phys. Rev. Lett. **124**, 101101 (2020).
[48] J. Millen, T. S. Monteiro, R. Pettit, and A. N. Vamivakas, Rep. Prog. Phys. **83**, 026401 (2020).
[49] D. C. Moore and A. A. Geraci, Quantum Sci. Technol. **6**, 014008 (2021).
[50] F. Monteiro, W. Li, G. Afek, C.-l. Li, M. Mossman, and D. C. Moore, Phys. Rev. A **101**, 053835 (2020).
[51] G. Ranjit, D. P. Atherton, J. H. Stutz, M. Cunningham, and A. A. Geraci, Phys. Rev. A **91**, 051805(R) (2015).
[52] G. Bimonte, Phys. Rev. D **98**, 105004 (2018).
[53] A. L. Erickcek, N. Barnaby, C. Burrage, and Z. Huang, Phys. Rev. D **89**, 084074 (2014).
[54] A. Padilla, E. Platts, D. Stefanyszyn, A. Walters, A. Weltman, and T. Wilson, J. Cosmol. Astropart. Phys. 03 (2016) 058.
[55] A. L. Erickcek, N. Barnaby, C. Burrage, and Z. Huang, Phys. Rev. Lett. **110**, 171101 (2013).
[56] A. Upadhye, W. Hu, and J. Khoury, Phys. Rev. Lett. **109**, 041301 (2012).
[57] C. Timberlake, G. Gasbarri, A. Vinante, A. Setter, and H. Ulbricht, Appl. Phys. Lett. **115**, 224101 (2019).
[58] F. Xiong, P. Yin, T. Wu, H. Xie, R. Li, Y. Leng, Y. Li, C. Duan, X. Kong, P. Huang, and J. Du, Phys. Rev. Applied **16**, L011003 (2021).
[59] C. W. Lewandowski, T. D. Knowles, Z. B. Etienne, and B. D'Urso, Phys. Rev. Applied **15**, 014050 (2021).
[60] C. Brown, Y. Wang, M. Namazi, G. Harris, M. Uysal, and J. Harris, arXiv:2109.05618.
[61] C. Miller and A. L. Erickcek, Phys. Rev. D **94**, 104049 (2016).
[62] C. Burrage, E. J. Copeland, A. Moss, and J. A. Stevenson, J. Cosmol. Astropart. Phys. 01 (**2018**) 056.